Chinese Chemical Letters 33 (2022) 1346–1352

Contents lists available at ScienceDirect

Chinese Chemical Letters

journal homepage: www.elsevier.com/locate/cclet

Fe doped aluminoborate PKU-1 catalysts for the ketalization of glycerol to solketal: Unveiling the effects of iron composition and boron

Weilu Wang[a,*], Xiangke Zeng[a], Yanliu Dang[b], Ping Ouyang[a], Haidong Zhang[a], Guangming Jiang[a], Fan Dong[a,c], Tao Yang[d], Steven L. Suib[b], Yang He[e,*]

[a] Engineering Research Center for Waste Oil Recovery Technology and Equipment, Ministry of Education, Chongqing Technology and Business University, Chongqing 400067, China
[b] Institute of Materials Science, University of Connecticut, Storrs, CT 06269, United States
[c] Yangtze Delta Region Institute (Huzhou) & Institute of Fundamental and Frontier Sciences, University of Electronic Science and Technology of China, Huzhou 313001, China
[d] College of Chemistry and Chemical Engineering, Chongqing University, Chongqing 401331, China
[e] Department of Chemical, Biological and Materials Engineering, University of South Florida, Tampa, FL 33620, United States

ARTICLE INFO

Article history:
Received 8 May 2021
Revised 30 July 2021
Accepted 11 August 2021
Available online 16 August 2021

Keywords:
Fe doping aluminoborate
Glycerol recycling
Ketalization
Boron reaction sites
Lewis-acid dominating catalyst

ABSTRACT

An inexpensive Fe doped aluminoborate consisted of 18% Fe in PKU-1 material that exhibits high selectivity of 4-hydroxymethy-2,2-dimethyl-1,3-dioxolane (Solketal, 98.3%), considerable activity (TOF 51.7 h^{-1}), and recyclable ability in the ketalization of glycerol to Solketal with acetone at 318 K has been developed. Our study demonstrated that the structure of Fe (less agglomerated iron species *vs.* FeO_x clusters) can be tuned by changing Fe loading in the PKU-1 material, which correlated well with experimental observations. Furthermore, the surface boron sites were promoted by iron loading and behaved as Lewis-acid sites to facilitate the reaction process of glycerol ketalization, while the Solketal selectivity was closely related with the structure of iron species in PKU-1, which was proved by kinetic studies, density function theory (DFT) calculations, and a series of spectroscopy studies. This investigation demonstrates that the surface B sites can play important roles in the reaction instead of being spectators.

In the last few decades, much effort has been made to find alternatives for fossil fuels. Biofuels, particularly as biodiesel, have attracted extensive attention due to such green energy sources [1-5]. Glycerol (GLY) is one of the main products from the reactions of biodiesel. The global production of GLY is about 5.2 million tons in 2020, and the crude glycerol price is currently as low as 0.04-0.09 $/lb [6]. Therefore, it is of importance and economical interest to develop selective catalysts to upgrade GLY into renewable fuels and valuable chemicals. Solketal is a critical and valuable chemical that can be used as an additive to decrease the viscosity, improve cold properties, provide the flash point, and increase the octane number of fuels [7-9]. Solketal also can function as an intermediate to synthesize high-value compounds, such as propylene glycol, quinolines, and higher aldehydes through transacetalization reactions [10,11].

In general, Solketal is produced *via* an acid-catalyzed mechanism in the ketalization reaction where the soluble acids (*i.e.*, HCl, H_2SO_4 and *p*-toluenesulfonic acid) were used as catalysts. However, these mineral acids are not recyclable, uneconomical, and environmentally damaging [12,13]. An alternative strategy to circumvent the above mentioned disadvantages is to perform the reaction in a heterogeneous catalysis system. Published work has shown that both Brønsted and Lewis acid sites in solid acids played important roles in the ketalization reaction. For instance, Sn and Fe have been applied as Lewis acid sites (LAS) to activate the carbonyl group in acetone to form electrophilic centers, which facilitated the reaction process towards Solketal (4-hydroxymethy-2,2-dimethyl-1,3-dioxolane), Dioxane (2,2-dimethyl-1,3-dioxan-5-ol) and water [14,15]. In the case of Brønsted acid sites (BAS), a tertiary alcohol was generally formed at the beginning over the terminal hydroxyl group of GLY and the carbonyl group of acetone by the activation and thus generate final product [6]. A few studies also suggest that the first step of glycerol acetalization occurred in the presence of BAS, which activates the carbonyl group in acetone in the first step

* Corresponding authors.
E-mail addresses: weiluwang@ctbu.edu.cn (W. Wang), yangh1@usf.edu (Y. He).

https://doi.org/10.1016/j.cclet.2021.08.056
1001-8417/

[6,14]. More effects have been adopted to obtain catalysts with satisfactory BAS rather than the ones involving perfect Lewis acidity due to the low capacity of LAS to convert the acetone-glycerol adduct to final products and poor water resistance [6,16].

Fe-promoted porous materials have been extensively studied due to their high activity in the reactions involving CO_x, NO_x, and CH_x groups, especially the catalytic effect caused by the physichochemical properties of iron composition, such as aggregation extent and valence state [17–25]. These iron species also can function as Lewis acid sites to control over the adsorption of reactants and products, and thus modify reactivities of catalysts. Tiago Pinheiro Braga reported that $CoFe_2O_4$-MCM-41 catalyzed the dehydrogenation of ethylbenzene to styrene with high efficiency due to potent activation of ethylbenzene by the Lewis-acid FeO_x groups in molecular sieve [26]. Additionally, isolated Fe^{3+} in Beta zeolite can enhance the surface acidity, and thus to improve the reaction performance of NO_x-SCR by modulating NH_3 adsorption [27]. The activity of Fe composition can be further elevated in incorporating with the non-metal elements, *i.e.*, N and P, and presents remarkable reactivity in CO_2 reduction [25], oxygen reduction reaction [28] *etc*. The non-metal element, boron was attractive due to its electron deficiency and Lewis acidity, but traditionally considered as a spectator rather than participating in the reaction [29,30]. More studies have shown that the boron element is active in some reactions. For instance, Hermans and co-workers have shown that the species formed by B and O in BN material played a critical role in oxidative dehydrogenation of propane [31]. Li-Yuan Zhao *et al.* also suggested that B_2O_3 was Lewis-acid active for the ring-opening process of epoxides [32]. The surface chemistry can be further modified when these BO_x groups combined with other functional groups, *e.g.*, hydroxyl groups, and transition metals in a number of reactions [33–36].

These years, a unique series of transition-metal doped aluminoborate catalysts has been investigated, named as *M*-PKU-n, consisting of AlO_6 octahedra and borate groups by sharing vertex oxygen atoms. The catalysts possess multi-ring channels that enable the accommodation of high levels of transition metals, and have been shown to exhibit excellent catalytic performance in the reactions of selective oxidation of alcohols [37], dehydrogenation of styrene [38], and the Strecker reaction [35]. However, the roles of transition metal and boron sites in the catalytic process still remained unclear.

Herein, a suite of Fe-promoted PKU-1 ($HAl_3B_6O_{12}(OH)_4 \cdot nH_2O$) was investigated by systematically increasing Fe composition to ascertain the roles of Fe and B atoms in the ketalization reaction. Our study demonstrated how the catalytic reactivity could be influenced by the existence of Fe composition in the ketalization reaction. The surface B atoms that behave as Lewis-acid sites exhibit an aggressive reactivity towards acetone instead of being spectators. These novel findings are supported by catalytic performance tests, density function theory (DFT) calculations, and a series of spectroscopy studies.

To understand if the crystal structure of PKU-1 is affected by doped Fe, a systematic XRD study was performed as a function of Fe loading (Fig. 1a). The results showed no clear change in the XRD patterns of PKU-1 as Fe loading increased from 0 to 30%, which suggested Fe did not change the bulk structure of PKU-1. Besides, enlargements of crystal data, such as cell volume (Fig. 1b), *a*-axis, and *c*-axis (Fig. S1 in Supporting information), obtained by Lebail Refinement supports the fact that Fe atoms have a larger radius (0.645 Å, coordination number (CN) = 6) than Al atoms (0.535 Å, CN = 6) [39]. A linear increase in cell volume was found as the Fe loading increased, while a plateau was achieved when Fe loading above 18%. As shown in IR spectra (Fig. S2), the broad absorption bands at around 1626 and 2750-3700 cm^{-1} are related to the stretching vibrations of O−H groups [40]. The band peaks appear at 586 and 624 cm^{-1}, corresponding to vibration movements of Al-O bonds in octahedron [41]. The others were located at ~490, 713, 893, 948 and 1340 cm^{-1} are attributed to the B-O antisymmetric stretch, while the last four were related to BO species in [BO_3] groups [40]. The absence of characteristic peaks at ~1018 and 853 cm^{-1} corresponding to [BO_4] groups indicates that the boron atom has taken the planar triangle [BO_3] coordination mode rather than the tetrahedral [BO_4] one [42]. It can be suggested in these IR patterns that Al atoms were also exclusively in octahedral coordination, while the B atoms were also coordinated in triangular geometries as ferric species increased in framework, which further indicated that Fe dopant did not change the framework of PKU-1. These data provided convincing evidence for the successful isomorphous substitution of ferric iron into the lattice of PKU-1 when Fe loading was lower than 18%. Some more famous molecular sieve, such as Fe-ZSM-5 and MCM-41, consisted of tetrahedral-based framework. Their unit cell parameters generally show unobvious change by transition metal (TM) doping due to extra-framework insertion or low-concentration-type incorporation in the framework [43,44]. Thus, the advanced reactivity of these materials promoted by framework substitution was often doubtful and cannot be conclusive.

The calculations based on the Scherrer equation toward XRD patterns was also applied to estimate the mean crystallite sizes of these metal-borates, which showed that a small rise in crystallite size is observed by increasing the Fe loading in samples (Fig. 1b and Table S2 in Supporting information). This situation was also verified by the specific surface areas of 10% PKU-1, 18% Fe-PKU-1, and 25% Fe-PKU-1, *i.e.*, 89.4, 61.4 and 45.2 m^2/g (Fig S3 in Supporting information). The water contact angles (WCAs) of PKU-1, 4% Fe-PKU-1, 10% Fe-PKU-1, 18% Fe-PKU-1, 20% Fe-PKU-1 and 25% Fe-PKU-1 are 10.9°, 12.1°, 21.7°, 31.9°, 24.4°, and 22.7° (Fig. 1d and Fig. S4 in Supporting information), suggesting that Fe doping was a benefit to improve the degree of hydrophobicity for PKU-1, whereas these Fe promoted metal-borates were getting more hydrophilic if iron composition exceeded 18%.

The morphology and chemical composition of Fe-PKU-1 samples were analyzed by TEM and ICP. In TEM images (Fig. 1b), the 18% Fe-PKU-1 catalyst exhibited a needle-like morphology, and the EDS elemental mapping analysis (Fig. 1d) suggested the homogeneous distribution of Al and Fe species all over the sample. Additionally, the lattice fringes and diffraction spots (Fig. S5 in Supporting information) from HRTEM indicated the presence of single crystals with well-defined (110) and (100) facets. As shown in Fig. 1b, the ICP-AES results showed that the actual Fe loading was within a few percent of target loading over all Fe-PKU-1 catalysts.

To reveal the elemental composition and electronic structure presented in the near surface layers of *x* Fe-PKU-1, XPS measurements were performed over Fe-PKU-1 catalysts with 0%, 10%, 18%, and 20% Fe loadings. Figs. 1c, and e and Fig. S6 (Supporting information) showed the detailed regions of Al 2p, Fe 2p, B 1s, and O 1s. The full XPS spectra are shown in Fig. S7 (Supporting information). The binding energy (BE) of C 1s peak at 284.6 eV was taken as a reference. The results showed that the Fe $2p_{3/2}$ and $2p_{1/2}$ peaks of 18% Fe-PKU-1 were at 712.5 and 725.9 eV, respectively, which were clearly higher than Fe_2O_3 (710.9 eV and 724.5 eV). This could be attributed to the high dispersion of Fe atoms within the PKU-1 framework [45,46]. Both Fe 2p peaks were systematically shifted towards lower BE while the Al 2p and B 1s peaks shifted to higher BE. This suggested a strong electronic interaction between iron, aluminum, and boron. This strong electronic interaction was also evidenced by the systematic peak shift of O 1s towards lower BE as Fe composition increased (Fig. S6b). This shift may suggest an increase in the amount of surface oxygen vacancies when the Fe composition was elevated, which facilitated the electron transfer from Al and B to Fe [47]. The similar BE shifts of Fe 2p and

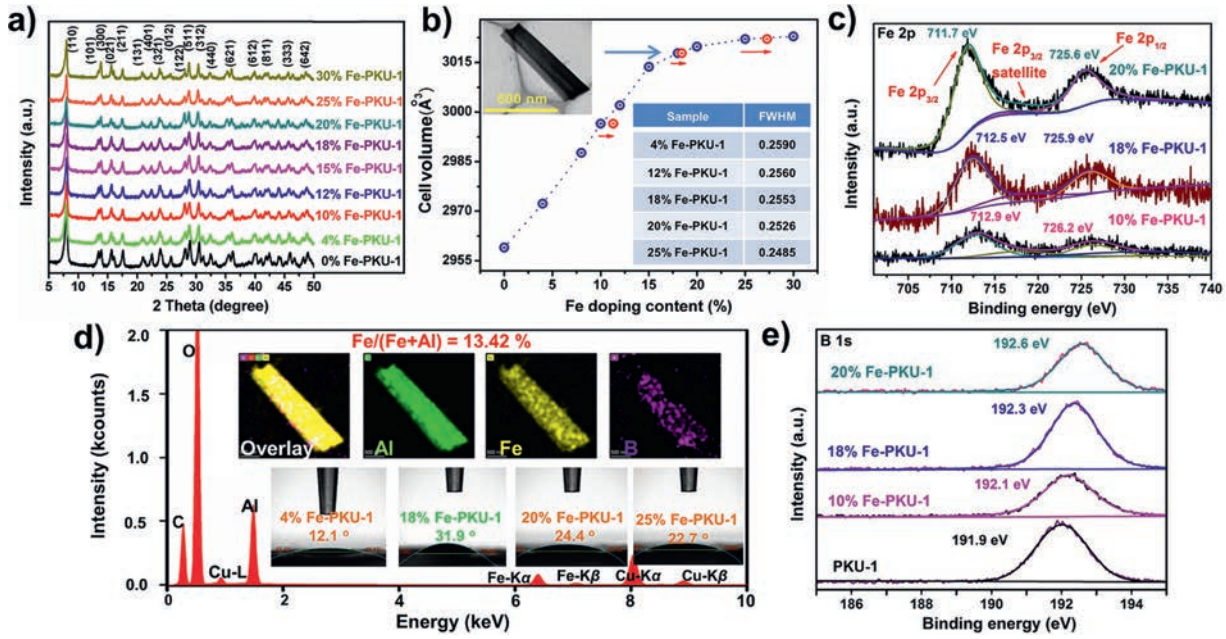

Fig. 1. (a) Powder XRD patterns for *x* Fe-PKU-1 samples (*x* = 0%, 4%, 10%, 12%, 15%, 18%, 20%, 25% and 30%). (b) Cell volumes obtained by Le Bail fitting *vs. x* (the blue dots). The red dots represent the calculated *x* values from ICP-AES experiments; TEM images for 18% Fe-PKU-1 and crystallite sizes of these samples based on (110) lattice planes were inset. (c) XPS spectra for Fe 2p of 10% Fe-PKU-1, 18% Fe-PKU-1 and 20% Fe-PKU-1. (d) The EDS elemental mapping of Fe, Al, and B. Contact angles measurements of 4% Fe-PKU-1, 18% Fe-PKU-1, 20% Fe-PKU-1 and 25% Fe-PKU-1 were inset. (e) XPS spectra for B 1s of PKU-1, 10% Fe-PKU-1, 18% Fe-PKU-1 and 20% Fe-PKU-1.

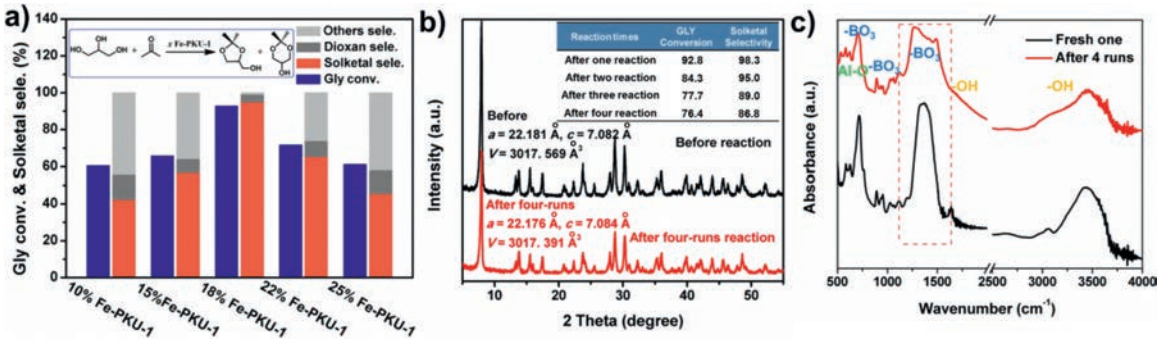

Fig. 2. (a) Catalytic performance of Fe-PKU-1 with different Fe loading over the ketalization reaction. (b) The recyclability of 18% Fe-PKU-1 for GLY ketalization and its powder XRD results before and after four-run reaction. (c) IR spectra of 18% Fe-PKU-1 before and after four-run reaction.

O 1s in the *x* Fe-PKU-1 materials also suggested that both Fe and O atoms obtained electrons from the surrounding Al and B atoms. The charge transfer can modulate the surface acid-base properties of catalysts and further influence their reactivity.

Catalytic performance was then measured over all Fe-promoted alminoborates to investigate the specific function of the incorporated iron element in ketalization reactions. All tests were performed in a 50 mL flask heated by a silicon oil bath under vigorous stirring with 400 rmp/min. As shown in Fig. 2a, a steady increase in the reaction performance of GLY ketalization was found as the Fe loading increased. However, both conversion and Solketal selectivity dropped, and the side reactions were simultaneously promoted when Fe loading exceeded 18% in PKU-1. Thus, ferric incorporation does not always help to improve the catalytic reactivity of PKU-1. Perhaps the surface hydrophobicity-hydrophilicity of catalysts changes as Fe doping increasing, which property was claimed to result in the variation over their catalytic activity towards GLY ketalization [8]. As shown in Fig. 1d, the hydrophobicity of PKU-1 gradually increased with the iron content in the material, however these Fe promoted metal-borates were getting more hydrophilic if iron composition exceeded 18%. The hydrophobicity of catalysts was demonstrated to accelerate the dehydration step of the intermediate formed from glycerol and ketones, and thus facilitate the ketonization reaction of GLY [6]. The deeper reasons will be discussed later. When benzaldehyde was applied to react with GLY, and the conversion was trace. So, relatively large reactants may not easily access the surface reaction site in catalysts. Ganapati V. Shanbhag and colleagues reported similar reaction results, which also suggested the ketones in smaller-sized reacting with glycerol were favored to form Solketal rather than Dioxane products [48]. In addition, as suggested before, Fe doping enhances the crystallinity of PKU-1 and the surface area of these Fe promoted alumino-borates is also correspondingly reduced. Thus, Fe loading in PKU-1 does not always help to enhance the catalytic activities.

The reaction temperature was also varied to investigate the effect on catalytic performance. Our results showed that the ketalization reaction could be promoted as the temperature increased up to 318 K whereas the Solketal selectivity dropped significantly when the temperature was above 318 K (Fig. S8a in Supporting information). This phenomenon could be due to the exothermic nature of the glycerol acetalization reaction. This slight decrease is consistent with previous studies over the batch reaction system

Table 1
Comparison of GLY ketalization with previously reported LAS dominating catalysts.

Catalyst	Reaction temp. (K)	Reaction time (h)	GLY conv. (%)	Solketal sel. (%)	Facial TOF[a] (h^{-1})	Initial TOF[b] (h^{-1})	Ref.
Hf-TUD-1	353	6	52	> 99	320	—	[51]
V-MCM-41	333	1	~ 93	~ 95	0.18	—	[52]
VO_xNT	383	6	73	17	37	—	[53]
Fe-PKU-1	318	3	92.8	98.3	51.7	358.4	This work

[a] Facial TOF was calculated by the expression [converted substrate]/{[mole of acidic sites in catalyst]*time} and according to the reaction data at 3 h (h^{-1}).
[b] Initial TOF was calculated based on the methods plotted in Fig. S9.

Table 2
The chemical composition of surface elements in *x* Fe-PKU-1.

Catalyst	Atomic ratio (%)			Fe/(Fe+Al+B) ratios (%)	Atomic concentration (%)		
	Fe	Al	B		O_L	O_{ads}	O_{H2O}
PKU-1	0	10.3	23.4	—	3.5	39.3	57.2
10% Fe-PKU-1	0.9	10.2	22.7	2.6	7.6	39.6	52.5
18% Fe-PKU-1	1.3	9.3	21.5	4.0	9.2	39.6	48.8
20% Fe-PKU-1	1.6	9.1	19.1	5.4	9.9	39.4	50.7

[8]. As shown in Fig. S8b (Supporting information), the steady increase of catalyst loading (18% Fe-PKU-1) was beneficial to improve GLY translation and the selectivity of Solketal. However, a further enhancement of Solketal yields could not be achieved if the catalyst loading was more than 50 mg due to more acidic sites are not conducive to the process of GLY acetalization. As for the feed ratio of glycerol and acetone (Fig. S8c in Supporting information), a similar trend was displayed and the optimal ratio was 1/5. Moreover, 18% Fe-PKU-1 could be recycled up to four times (Fig. 2b inset) with a 17.7% decrease in catalytic performance. This could be caused by the occupation of surface reaction sites by strongly bound reactants or intermediates [8,49,50]. After 4 runs, 18% Fe-PKU-1 gave almost the same XRD pattern in comparison to the as-synthesized one. The crystal parameters of 18% Fe-PKU-1, *a, c* and *V*, were almost identical even after 4 runs (Fig. 2b inset), which suggested a highly stable framework with Fe dopants, while the IR results of the fresh sample and the recycled material showed a difference which is related to BO_3 groups (Fig. 2c). Fe-PKU-1 was superior in conversion (92.8%, corresponds to 93.7% of theoretical maximum 99.0%), selectivity (98.3%), and TOF (358.4 h^{-1}, initial; 51.7 h^{-1}, facial) in comparison to other Lewis-acid catalysts reported in recent years (Table 1). These catalysts were also reported to suffer from lower GLY conversion, Solketal selectivity, and unsatisfactory activity [51–53].

To get insight into the effect of surface compositional changes on the catalytic reactivity of Fe-PKU-1, the chemical constitution of the material surface was analyzed. Our XPS results showed that the surface Fe composition was gradually increased while the composition of B was lowered when Fe loading increased (Table 2). This phenomenon was also encountered in the published work [54–56]. Combined with the above catalytic results (Fig. 2a), this suggested that the systematic increase in the surface Fe composition could promote the selectivity of Solketal when the total Fe loading was equal or less than 18%. However, the drastic drop of Solketal selectivity indicated a change in surface reactivity when the total Fe loading was higher than 18%. The deconvolution of the O 1s core level (Fig. S6b) from XPS measurements showed several different types of O species, which were lattice oxygen (O_L, 529.7 eV), surface chemisorbed hydroxyl groups or other surface oxide species (O_{ads}, 531.3 eV), and molecular water adsorbed on the surface (O_{H_2O}, 532.8 eV), respectively [57,58]. Table 2 also shows that the composition of O_L was drastically increased when the Fe loading was below 18%, and little change of O_{ads} indicated the relative stability of the BAS amount in the Fe-PKU-1 surface. However, little change of O_L was found when the Fe loading exceeded 18%. The well-dispersed Fe species within PKU-1 could form small clusters as the Fe loading increased to a certain level, which may be related to the decrease in conversion and Solketal selectivity. This hypothesis will be discussed in detail in the following paragraph.

UV-vis diffuse spectroscopy was employed to analyze the charge transfer transitions between Fe and O within Fe-doped PKU-1 catalysts with 10%, 18%, 20% and 30% Fe compositions, which can provide information on the coordination states and extent of aggregation of iron species within the catalysts [19]. Band deconvolution was performed by Gaussian/Lorentz functions to get insight into the Fe species within the catalysts. The results showed a pronounced adsorption band around 270 nm over all Fe-doped PKU-1 materials, which could be attributed to the isolated six-coordinated Fe-O vibrations [59,60]. This band was broadened as Fe composition increased (Fig. S10 in Supporting information). All catalysts displayed a fitted peak between 300 and 400 nm, which could be due to the formation of small oligomeric iron clusters [61]. This coincided with the observation of increased Fe composition near the surface *via* XPS measurements as Fe loading increased (Table 2). The peak area of adsorption bands above 400 nm was small originally, which was assigned to d-d transitions of large Fe_2O_3 particles located at the external surface of the catalyst [61,62]. Quantitative analysis (Table 3) showed that Fe was initially in the form of less agglomerated iron species ($\lambda < 300$ nm), within PKU-1 bulk, and oligomerized to clusters (300 nm $< \lambda <$ 400 nm) as the composition increased. Finally, large Fe_2O_3 particles ($\lambda >$ 400 nm) were formed when Fe composition exceeded 18%. The formation of large Fe_2O_3 particles appeared to reduce the surface reactivity, which may correspond to the decrease in GLY conversion and Solketal selectivity.

The nature of catalyst acidity has been shown to play critical roles in dictating catalytic reactivity in ketalization reaction [6,63,64]. The acidic properties of these Fe containing aluminoborates were investigated using nonaqueous potentiometric titrations with *n*-butylamine in acetonitrile. The total amount of acidic sites and E_i values (corresponding to the strength of acid sites) of *x* Fe-PKU-1 were calculated based on the potentiometric titration curves (Fig. 3a). The results showed a volcano trend between E_i values and Fe compositions, 18% Fe-PKU-1 also displayed the highest E_i value (99.1 mV). This coincided with the trend observed in the catalytic performance tests, which suggested that the enhanced acidity of the catalyst could improve the catalytic performance in the ketalization reaction. Quantitative analysis showed that the amounts of acid sites were 0.031, 0.032, 0.065, 0.039 and 0.036 mmol/g for PKU-1, 12% Fe-PKU-1, 18% Fe-PKU-1, 22% Fe-PKU-1 and 25% Fe-

Table 3
Percentages of different iron species calculated from the deconvolution of UV-visible diffuse reflectance spectra of Fe-PKU-1.

Catalyst	Fe species (%)		
	I_1 (%, λ < 300 nm)	I_2 (%, 300< λ < 400 nm)	I_3 (%, λ > 400 nm)
10% Fe-PKU-1	71.4	23.7	4.9
18% Fe-PKU-1	64.9	24.4	10.7
20% Fe-PKU-1	47.9	25.4	26.7
30% Fe-PKU-1	38.3	30.3	31.4

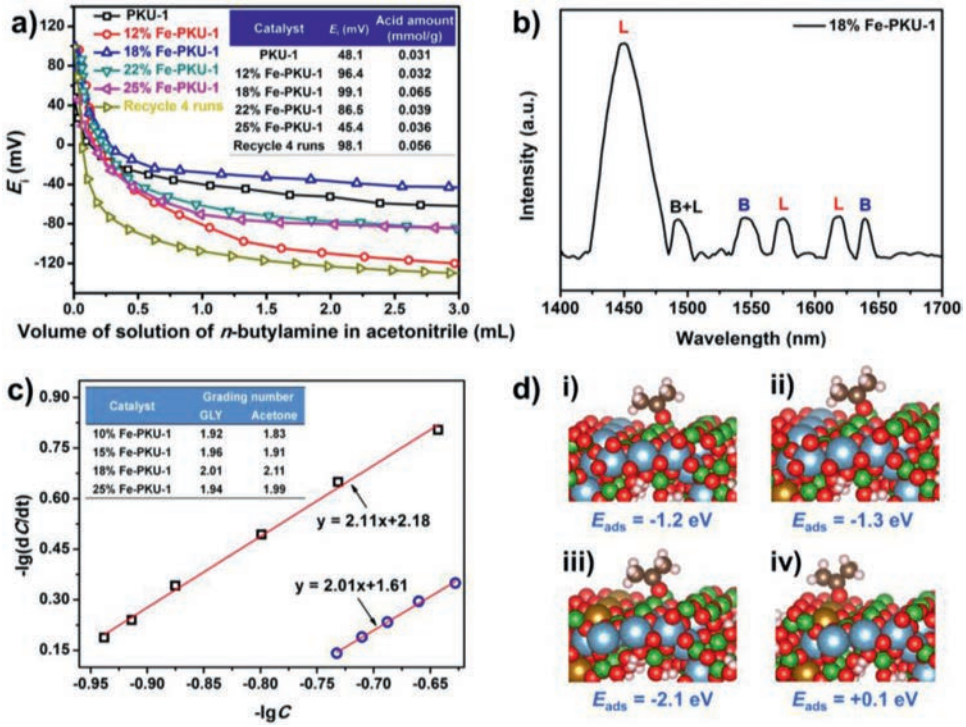

Fig. 3. (a) Potentiometric titration employing *n*-butylamine for PKU-1 with different Fe loading and the test results were also shown inset. (b) The result of Pyridine-IR measurement for 18% Fe-PKU-1. (c) Kinetic studies of GLY and acetone catalyzed by Fe-PKU-1: plots of $-\lg(dC_{GLY\ or\ acetone}/dt)$ *vs.* $-\lg(C_x)$. The grading numbers of GLY and acetone over PKU-1 with 10%, 15%, 18% and 25% Fe loading were inset. (d) Acetone adsorption on (i) the boron site of pure PKU-1, (ii) the boron site of PKU-1 modified with the Fe in the lattice, (iii) the boron site and (iv) the Fe site of PKU-1 modified with Fe both in the lattice and on the surface. Green sphere, B; red sphere, O; blue sphere, Al; light pink sphere, H; light brown sphere, Fe; dark brown sphere, C.

PKU-1, respectively. The 18% Fe-PKU-1 catalyst possesses the highest amount of acid sites and thus the highest catalytic reactivity was obtained (Fig. 3a inset). It is worth noting that the E_i values of 18% Fe-PKU-1 slightly decreased from 99.1 eV to 98.1 eV after 4 runs reaction, whereas the amount of acid sites in this sample fell by 10%, thus the latter was more related to the loss for reaction activity (17.7%) of this sample. Thus, the acid amounts in Fe-PKU-1 are more necessary than the strength of acid sites for facilitating this reaction process.

To further ascertain the role of Brønsted and Lewis acid sites in the GLY ketalization reaction mechanism over this kind of catalytic materials, FT-IR with pyridine adsorption was applied to test acid properties of 18% Fe-PKU-1. As shown in Fig. 3b, peaks located at 1449, 1574 and 1617 cm^{-1} are ascribed to Lewis acid sites; 1544 and 1639 cm^{-1} was linked to BAS sites caused by B-OH. The 1491 cm^{-1} band are corresponding to the contribution of both LAS and BAS. It is clear that more LAS present in the sample of 18% Fe-PKU-1 than BAS. As suggested before, XPS results showed little change in O_{ads}, indicating the relative stability in BAS amount in these Fe promoted alumino-borates surface. The XPS results also showed that electrons were transferred from Al and B to O and Fe with iron doping rising, and this electron loss in boron atoms can enhance its Lewis acid nature. In addition, Fe species was proved to be doped into the lattice of PKU-1 successfully, and the UV-vis test indicated they could change from isolated atoms to binuclear and small clusters in the material. This variation could influence the physio-chemical properties of Fe species such as its Lewis acid nature, and improve its catalytic activity [65]. Therefore, kinetic studies and DFT was applied to ascertain the contribution of iron and boron for their Lewis acid properties in the reaction process in the following paragraphs. Further combining with BET measurements of these Fe promoted alumino-borates (Fig. S3) and the previous views about the channel blocking of PKU-1 with boric acid [66], it can be inferred that the reaction occurs on the geometric surface of Fe-PKU-1, and the catalytic effects were related to acid sites in Fe-PKU-1 exclusively rather than the specific surface area of catalysts.

Kinetic experiments and related time-varying reactions were also designed to further obtain some enlightenment about the reaction mechanism. The kinetic parameters of the reaction were calculated based on the mathematical operations of experimental data at different times over the 18% Fe-PKU-1 catalyst. The results showed a good linear relationship between $\ln(dC_{GLY}/dt)$ and $\ln(C_{GLY})$ when the concentration of GLY was extremely high (10.0 mol/L) in the reactant solution (Fig. 3c). A similar trend was also found when excess acetone was applied in the reaction. The slopes

of the correlation between $\ln(dC_x/dt)$ and $\ln(C_x)$ for these two cases were measured as 2.01 and 2.11, respectively, which indicated that the ketalization reaction over 18% Fe-PKU-1 obeyed second-order reaction kinetics [67]. To understand how Fe affected the kinetics in the reaction, the grading numbers of GLY and acetone were investigated as a function of Fe composition in the PKU-1 framework. Figs. S11 and S12 (Supporting information) showed that the grading number of GLY varies from 1.92 to 2.01 with Fe/(Fe+Al) ratio rising from 10% to 25%, while the ones of acetone increased from 1.83 to 2.11. The results suggested that these metal-borates favored the activation of acetone more than GLY.

It is also critical to understand the role of boron sites of *x* Fe-PKU-1 in the reaction. Our prior study on PKU-1 indicated that the boron atoms could behave as Lewis acid sites in the Strecker reaction. These sites could also work with their adjacent hydroxyl groups that behave as Brønsted acid centers in the reaction [66]. The Lewis acid sites were more favored in activating acetone than the Brønsted acid sites [51]. In the current study, the kinetic results indicated that acetone was more sensitive than GLY in the ketalization reaction over *x* Fe-PKU-1 catalysts (Fig. 3c). Therefore, quantum chemical modeling calculations were employed using acetone as a probe to ascertain if the surface B reaction sites have higher reactivity towards acetone. Surface Fe sites were also tested for comparison since they could also behave as the Lewis acid sites. We have modeled pure PKU-1, Fe-doped inside the lattice of PKU-1, and Fe doped into the lattice and on the surface of PKU-1 in this study (Fig. 3d). In the case of pure PKU-1, the adsorption energy of acetone on the boron sites was calculated as −1.2 eV. The energy became slightly exothermic when Fe was incorporated into the PKU-1 lattice (E_{ads} = −1.3 eV), which suggested a minor effect on acetone bonding strength when Fe composition was too low. However, the interaction between surface boron sites and acetone molecule was drastically increased when Fe was present on the surface (−2.1 eV), which indicated a significant improvement in the surface reactivity of boron reaction sites. This could be attributed to the change of the electronic structure of surface boron atoms when Fe species presented on the surface, which consisted of a blue shift in boron BE shown in XPS results (Fig. 1e). The enhanced surface reactivity of boron sites may facilitate the cleavage of C—O bond in the reaction. In comparison to the surface boron sites, the energy for acetone adsorption on the surface Fe sites was measured as +0.1 eV, which was much more endothermic than that on the boron sites. This distinguished energetic difference clearly indicated that the surface boron sites were more favorable to adsorb acetone than the surface Fe sites. This was also supported by our IR study over fresh and recycled catalysts where the peak related to the BO_3 group (1230-1575 cm^{-1}) broadens and splits after 4 runs, which suggests that the reactants are favored for bonding on surface boron sites (Fig. 2c). It is interesting to note that PKU-1 cannot facilitate GLY ketalization, while the reactivity of which were promoted if iron species was loaded into this material. Further combining with XPS result, it can be inferred that the charge transfer from B to ferric species may increase the Lewis acidity in boron atoms, and thus active acetone to accelerate the reaction process.

According to the obtained results and previous reports, a reaction mechanism was proposed and shown in Scheme 1. When the substrates diffused into the surface of Fe-PKU-1, the boron atoms function as LAS to active the propanone carbonyl groups in acetone, followed by the nucleophilic attack on the primary alcoholic group in GLY, accompanying with forming an intermediate by linking the β-carbon atoms of this triatomic alcohol. Then, the dehydration of this intermediate will take place and glycerol acetal forms finally. It is generally accepted that this dehydration was dominated by BAS, and could take a significant impact on the selectivity of Solketal [6]. However, in the current system, it seems

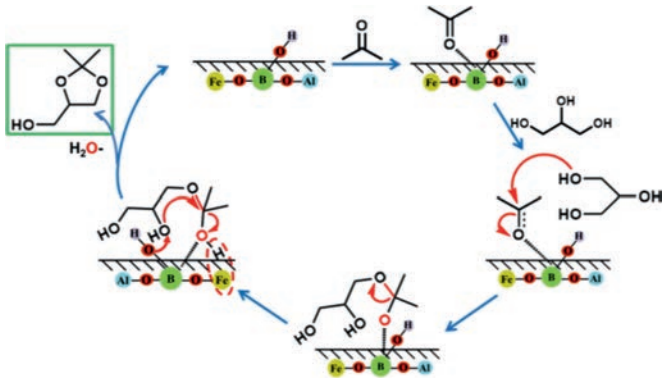

Scheme 1. Proposed mechanism for GLY ketalization catalyzed by Fe-PKU-1.

that Fe is more crucial for the generation of Solketal than BAS. Specifically, when iron species in low oligomeric are present simultaneously with BAS, the former is more closely related with Solketal formation. As reported previously, the catalogue of transition-metals, the valence and agglomerate extent which were reported to have a considerable influence on dehydration reactions. For example, the Fe-modified ZSM-5 displayed a higher catalytic performance than Cu-ZSM-5 for syngas to dimethyl ether process, due to a pronounced enhancement in the acid properties of ZSM-5 as ferric introduction [68]. In summary, the Solketal selectivity was suggested to closely relate with the structure-transformation of iron species in PKU-1, and boron species in PKU-1 could function as the Lewis-acid site to react with acetone to facilitate the ketalization reaction.

In conclusion, the reaction conversion was linearly increased when low content Fe dopant was dispersed in the lattice of PKU-1. However, the excess ferric composition (>18%) would translate to the ferric oxide, and the conversion and Solketal selectivity thus dropped. The catalyst of 18% Fe-PKU-1 was found to exhibit the best catalytic performance (92.8% conversion and 98.3% selectivity in Solketal). Furthermore, our XPS analyses, IR tests, acid-properties measurements, kinetic study, and DFT calculations all showed that boron sites played an important role for the activation of acetone to facilitate the reaction process, while the Solketal selectivity was closely related with the presence-state of iron species in PKU-1. It is worth noting that boron atoms in PKU-1 do not exhibit activity towards acetone, however, ferric introduction in PKU-1 material lead to a charge transfer between boron and iron dopants, *i.e.*, the electron loss in boron, which result in an enhancement in Lewis-acid nature in boron atoms and thus increase its reactivity. This finding is notable for the catalytic performance of boron atoms since they have been always treated as spectators in these reactions.

Declaration of competing interest

The authors declare that they have no financial and personal relationships with other people or organization that could have appeared to influence the work reported in this paper.

Acknowledgments

This work was financially supported by the Scientific and Technological Research Program of Chongqing Municipal Education Commission (Nos. KJQN202000823 and KJZD-K201900802), Research project of Chongqing Technology and Business University (No. 1956058), and Scientific Platform Project, Ministry of Education (No. fykf201905). S. L. Suib thanks the US Department of Energy Office of Basic Energy Sciences, Division of Chemical, Bio-

logical and Geological Sciences (No. DE-FG02-86ER13622.A000) for support of this research.

Supplementary materials

Supplementary material associated with this article can be found, in the online version, at doi:10.1016/j.cclet.2021.08.056.

References

[1] S.M. Huang, X.X. Kou, J. Shen, G.S. Chen, G.F. Ouyang, Angew. Chem. Inter. Ed. 59 (2020) 8786–8798.
[2] X.J. Wang, M. Hong, Angew. Chem. Inter. Ed. 59 (2020) 2664–2668.
[3] D. Ohayon, G. Nikiforidis, A. Savva, et al., Nat. Mater. 19 (2020) 456–463.
[4] K.E. You, S.C. Ammal, Z.X. Lin, et al., J. Catal. 388 (2020) 141–153.
[5] S.F. Zhao, W.D. Wang, L.Z. Wang, W. Wang, J. Huang, J. Catal. 389 (2020) 166–175.
[6] M.R. Nanda, Y.S. Zhang, Z.S. Yuan, et al., Renew. Sust. Energ. Rev. 56 (2016) 1022–1031.
[7] F.C. Ballotin, M.J. da Silva, A.P. de C. Teixeira, R.M. Lago, Fuel 274 (2020) 117799.
[8] M.S. Rahaman, T.K. Phung, Md.A. Hossain, et al., Appl. Catal. A: Gen. 592 (2020) 117369.
[9] K. Stawicka, A.E. Díaz-Álvarez, V. Calvino-Casilda, et al., J. Phys. Chem. C 120 (2016) 16699–16711.
[10] V.O. Samoilov, D.S. Ni, G.S. Dmitriev, L.N. Zanaveskin, A.L. Maximov, ACS Sustain. Chem. Eng. 7 (2019) 9330–9341.
[11] J. Jin, S. Guidi, Z. Abada, et al., Green Chem. 19 (2017) 2439–2447.
[12] V. Rossa, Y. da S.P. Pessanha, G.Ch. Díaz, et al., Ind. Eng. Chem. Res. 56 (2017) 479–488.
[13] C.X.A. da Silva, V.L.C. Gonçalves, C.J.A. Mota, Green Chem. 11 (2009) 38–41.
[14] M.J. Silva, A.A. Rodrigues, P.F. Pinheiro, Fuel 276 (2020) 118164.
[15] M.J. Silva, F.Á. Rodrigues, A.A. Júlio, Chem. Eng. J. 307 (2017) 828–835.
[16] A.W. Pierpont, E.R. Batista, R.L. Martin, et al., ACS Catal. 5 (2015) 1013–1019.
[17] Y.J. Zhu, B.B. Chen, R.R. Zhao, et al., Catal. Sci. Technol. 6 (2016) 6581–6592.
[18] P.F. Xie, Z. Ma, T. Meng, et al., J. Mol. Catal. A: Chem. 409 (2015) 50–58.
[19] G.J. Wu, F. Hei, N.J. Guan, L.D. Li, Catal. Sci. Technol. 3 (2013) 1333–1342.
[20] Y. He, S. Laursen, Catal. Sci. Technol. 8 (2018) 5302–5314.
[21] Y. He, S. Laursen, Surf. Sci. 686 (2019) 1–9.
[22] E.V. Kondratenko, J. Pérez-Ramıŕez, Appl. Catal. A: Gen. 267 (2004) 181–189.
[23] M. Mihaylov, E. Ivanova, K. Chakarova, P. Novachka, K. Hadjiivanov, Appl. Catal. A: Gen. 391 (2011) 3–10.
[24] B. Su, Z.C. Cao, Z.J. Shi, Acc. Chem. Res. 48 (2015) 886–896.
[25] A. Li, S.A. Nicolae, M. Qiao, et al., ChemCatChem 11 (2019) 1–25.
[26] M. da, C.B. Soares, F.F. Barbosa, M.A.M. Torres, et al., Catal. Sci. Technol. 9 (2019) 2469–2484.
[27] N. Zhu, Z.H. Lian, Y. Zhang, W.P. Shan, H. He, Chin. Chem. Lett. 30 (2019) 867–870.
[28] W. Wang, Q.Y. Jia, S. Mukerjee, S.L. Chen, ACS Catal 9 (2019) 10126–10141.
[29] X.M. Yu, P. Han, Z.X. Wei, et al., Joule 2 (2018) 1610–1622.
[30] C.W. Liu, Q.Y. Li, J. Zhang, et al., J. Mater. Chem. A 7 (2019) 4771–4776.
[31] J.T. Grant, C.A. Carrero, F. Goeltl, et al., Science 354 (2016) 1570–1573.
[32] L.Y. Zhao, J.Y. Chen, W.C. Li, A.H. Lu, J. CO_2 Util. 29 (2019) 172–178.
[33] W.L. Wang, C.M. Zeng, Y. Yang, et al., New J. Chem. 43 (2019) 18184–18192.
[34] S.X. Hu, W.L. Wang, M.F. Yue, et al., ACS Appl. Mater. Inter. 10 (2018) 15895–15904.
[35] W.L. Wang, S.Y. Zhang, S.X. Hu, et al., Appl. Catal. A: Gen. 542 (2017) 240–251.
[36] W.L. Wang, Y. He, J.K. He, et al., Catal. Sci. Technol. 11 (2021) 1365–1374.
[37] W.L. Wang, S.X. Hu, L.J. Li, et al., J. Catal. 352 (2017) 130–141.
[38] H.W. Chen, W.L. Wang, Y. Yang, et al., Appl. Catal. A: Gen. 588 (2019) 117283.
[39] F. Brulfert, J. Aupiais, Dalton Trans. 47 (2018) 9994-10001.
[40] G.J. Wang, W.L. Wang, F.H. Zhang, et al., Catal. Sci. Technol. 6 (2016) 5992–6001.
[41] H. Aydin, B. Elmusa, J. Aust. Ceram. Soc. 57 (2021) 731–741.
[42] J. Haber, V. Szybalska, Discuss. Faraday Soc. 72 (1981) 263–282.
[43] J.W. Harris, J. Arvay, G. Mitchell, W.N. Delgass, F.H. Ribeiro, J. Catal. 365 (2018) 105–114.
[44] W.B. Fan, R.G. Duan, T. Yokoi, et al., J. Am. Chem. Soc. 130 (2008) 10150–10164.
[45] J. Li, M. Zhao, M. Zhang, et al., Int. J. Chem. React. Eng. 18 (2019).
[46] M.C. Biesinger, B.P. Payne, A.P. Grosvenor, et al., Appl. Surf. Sci. 257 (2011) 2717–2730.
[47] G. Cheng, X. Liu, X.J. Song, et al., Appl. Catal. B: Environ. 277 (2020) 119196.
[48] P. Manjunathan, V.S. Marakatti, P. Chandra, et al., Catal. Today 309 (2018) 61–76.
[49] Y. He, S. Laursen, ACS Catal. 7 (2017) 3169–3180.
[50] Y. He, Y.J. Song, S. Laursen, ACS Catal. 9 (2019) 10464–10468.
[51] L. Li, T.I. Korányi, B.F. Sels, P.P. Pescarmona, Green Chem. 14 (2012) 1611–1619.
[52] T.H. Abreu, C.I. Meyer, C. Padró, L. Martins, Micropor. Mesopor. Mat. 273 (2019) 219–225.
[53] A.L.G. Pinheiro, J.V.C. do Carmo, D.C. Carvalho, et al., Fuel Process. Technol. 184 (2019) 45–56.
[54] Y. He, Y.J. Song, D.A. Cullen, S. Laursen, J. Am. Chem. Soc. 140 (2018) 14010–14014.
[55] Y.J. Song, Y. He, S. Laursen, ACS Catal. 10 (2010) 8968–8980.
[56] H.F. Xiong, S. Lin, J. Goetze, et al., Angew. Chem. Inter. Ed. 56 (2017) 8996 -8991.
[57] Q.T. Trinh, K. Bhola, P.N. Amaniampong, F. Jérôme, S.H. Mushrif, J. Phys. Chem. C 122 (2018) 22397–22406.
[58] Z. Li, Q.H. Yan, Q. Jiang, et al., Appl. Catal. B: Environ. 269 (2020) 118827.
[59] Q. Yuan, Q.H. Zhang, Y. Wang, J. Catal. 233 (2005) 221–233.
[60] M.S. Kumar, M. Schwidder, W. Grünert, A. Brückner, J. Catal. 227 (2004) 384–397.
[61] J.Y. Wang, H.A. Xia, X.H. Ju, et al., J. Catal. 300 (2013) 251–259.
[62] K.Q. Sun, H.A. Xia, Z.C. Feng, et al., J. Catal. 254 (2008) 383–396.
[63] S.S. Poly, Md.A.R. Jamil, A.S. Touchy, et al., Mol. Catal. 479 (2019) 110608.
[64] M.N. Moreira, R.P.V. Faria, A.M. Ribeiro, A.E. Rodrigues, Ind. Eng. Chem. Res. 58 (2019) 17746–17759.
[65] J. Zhu, F. Gao, L.H. Dong, et al., Appl. Catal. B: Environ. 95 (2010) 144–152.
[66] W.L. Wang, Y. Wang, B. Wu, et al., Catal. Commun. 58 (2015) 174–178.
[67] S.F. Lou, L.H. Jia, X.F. Guo, et al., RSC Adv. 6 (2016) 6921–6931.
[68] T.K.R.D. Oliverira, M. Rosset, O.W. Perez-Lopez, Catal. Commun. 104 (2018) 32–36.